Impedance evaluation of two-dimensional MEMS mirrors for failure analysis

Marlene Schneider[a], Norbert Druml[a], David Brunner[a], and Bernd Deutschmann[b]

[a]Infineon Technologies AG, Graz, Austria
[b]Institute of Electronics, University of Technology Graz, Graz, Austria

ABSTRACT

Microelectromechanical systems (MEMS) could be used for a large number of applications, like for example sensors, actuators, aerospace, health care, biomedical and automotive. The reliability analysis of two-dimensional (2D) MEMS mirrors is a rather new research area, where environmental and mechanical loads, like temperature and vibration, influence the operation of the mirrors, which may lead to fracture of the silicon structures. The aim of this work is to find out if it is possible to detect a breakage of 2D resonant MEMS mirrors by measuring their impedance. Therefore, a measurement setup was adapted to be able to perform a two-port measurement for the mirror with the help of a network analyzer. The results showed that the measurements are quite stable for different mirrors and that an impedance change for broken mirrors could be observed depending on the degree of breakage of the structures.

Keywords: 2D MEMS mirror, impedance measurement, failure analysis, reliability

1. INTRODUCTION

The realization of Microelectromechanical Systems (MEMS) mirrors was enabled by manufacturing advancement in the field of MEMS devices, where these mirrors are small-sized with a few square millimeter. Due to their ability to steer laser beams by controlling the direction and intensity of light,[1] they could be used for various automotive applications such as Head-Up Displays (HUD) and Light Detection and Ranging (LiDAR) sensors. Moreover, the steering of laser beams with the help of MEMS mirrors could be used for future augmented reality (AR) applications, such as AR googles.[2] MEMS mirrors could be implemented with two moving axes for a two-dimensional (2D) approach or with one moving axis (1D). For each case a control circuit is required, which operates the device and enables the beam steering, which is the MEMS driver application specific integrated circuit (ASIC).[3] For the actuation an electrostatic comb drive approach is used, where by applying a high voltage (HV) to the comb fingers, the capacitance structure applies an electric force that pulls the rotor towards its zero position.[4] The HV is switched on and off with a certain frequency in order to actuate the mirror.[2] A high mechanical quality factor (Q) is required to reach the desired oscillation angle, but at atmospheric pressure very high drive torques are needed. Therefore in order to overcome air damping vacuum packages are used.[5]

However, the reliability assessment of MEMS devices is a rather young research area with different failure aspects caused by environmental and mechanical loads, such as fatigue loads, mechanical vibration and shock, humidity and temperature, which lead to fracture of the structures. Moreover, non-linearity has to be taken into account for MEMS mirrors due to large displacements, stresses and the nonlinear properties of silicon, which is often used for MEMS devices.[6] In Ref. 7 the reliability of MEMS devices is described as the ability to perform their function without failure under defined conditions over a specified period of time. As some devices show life expectancies of billions of cycles, lifetime measurements could take quite long, which is problematic for research or post-production test. Therefore accelerated lifetime estimation is crucial in combination with applicable failure detection methods. There are existing optical methods with scanning electron microscopes (SEM) or laser interferometers, which allow reliable detection but are complicated to automate. On the other hand there are some electrical methods for MEMS switches, which rely on capacitance and resonant frequency variation measurements with complex implementation.[8]

E-mail: /marlenealexandra.schneider, norbert.druml, david.brunner/@infineon.com
marlene.schneider@student.tugraz.at, bernd.deutschmann@tugraz.at

In this paper a failure detection method for 2D electrostatic MEMS mirrors is investigated, which is based on evaluating the impedance with a two-port measurement with the help of a vector network analyzer (VNA). This measurement is executed for intact and broken mirrors without operation and the results are compared to each other with the goal to detect differences in the impedance for mirrors with broken structures. In addition, the capacitance of intact MEMS mirrors is determined and compared to simulation results.

2. IMPEDANCE MEASUREMENT OF MEMS MIRRORS

2.1 MEMS Mirror

The electrostatic actuation for the investigated 2D resonant MEMS mirror is based on the attraction of two oppositely charged plates, where comb actuation is preferred for high frequencies as this allows for larger motion and more evenly distributed forces. For the electrostatic comb drive actuation several plates are attached to each other like the fingers of a comb and form two rows, where one is static and the other is movable.[5] The movable row or rotor is pulled towards the static by applying a HV to the fingers and an electric force is generated by the capacitance structure.[4] The mechanical structures for 2D mirrors are fabricated with the help of deep reactive ion etching on silicon on insulator (SOI) wafers. The mirror is placed in the center and connected to two torsional springs, which are linked to a movable inner frame. The frame itself is linked to another pair of springs, which are connected to a fixed outer frame.[9] Moreover the comb fingers are perpendicular to the springs and are mounted on both sides of the mirror, while static comb fingers are placed on the substrate frames in order to attract the movable combs if a voltage is applied. By using oxide- or polysilicon-filled trenches the mirror is isolated from the frames and in order to set the structure free the backside silicon and buried oxide layer are detached.[10] Figure 1 shows the schematic view of the top layer of a typical 2D MEMS mirror as example.[11]

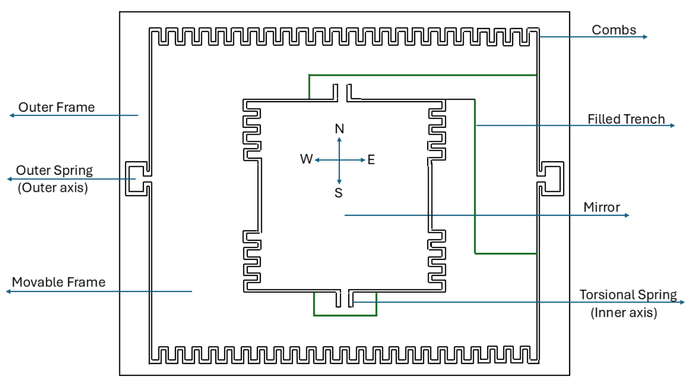

Figure 1. Schematic view of top layer of a typical 2D MEMS mirror with comb drive actuation.

The mechanical structure of the mirror enables a deflection in x- and y-direction with the two movable axes, which are referred to as outer and inner axis. In order to achieve Lissajous scanning, which is described in Ref. 5, the inner axis has a higher frequency and is the so called fast axis, while the outer axis is excited with a lower frequency and is called slow axis.[5]

2.2 Test Setup

In Fig. 2 the test setup for the two-port measurement is shown, which consists of a vector network analyzer (VNA), the MEMS mirror in a lead-less chip carrier (LCC) package as device under test (DUT), two 50 Ohm ports with SubMiniature version A (SMA) connectors, which are connected to different pads of the DUT and two SMA cables to connect the VNA to the ports. Moreover there is a ground plane (GND), which could be connected to different pads of the LCC package. The first port of the VNA was connected to the rotor pad for all tests, which was connected to the ground plane, while the second port was connected to the other pads for the different measurements. The pads of the LCC package are connected to the rotor pad of the mirror over the frames via interconnect poly tracks, which have a parasitic impedance.

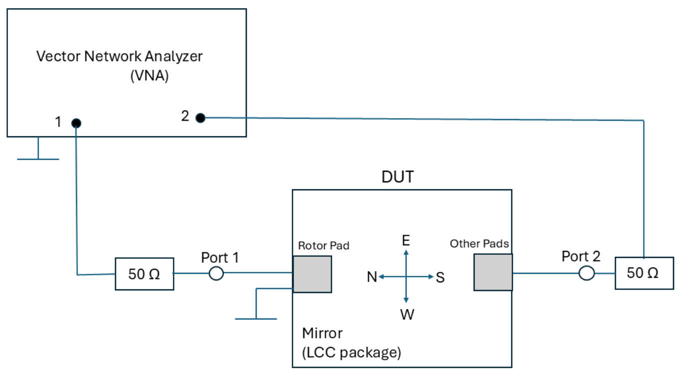

Figure 2. Test Setup for the two-port measurement with the mirror as DUT.

Table 1 gives an overview over the 11 pads of the MEMS mirror's LCC package for the two-port measurement. The rotor pad is located in the northern part of the package, while the measured pads are on the other sides and are used to drive and sense the combs of both mirror axes during operation. For the fast axis the northern combs, visible in Fig. 1, are connected to two of the fast axis sense pads on the east and west side, while the southern combs are connected to the drive pads located on the south side of the package and to the other two sense pads. The northern combs of the slow axis are connected to two of the slow axis sense pads on the east and west side and the southern combs are linked to the other two sense pads and to the drive pads on the south side. Moreover, there are simulation results available for the capacitance between different pads and the rotor pad, which could be compared to the measured results afterwards. For the results of the simulated capacitance C_{SIM} DC was assumed as they were extracted based on the geometry and layout.

Table 1. Pads of the MEMS mirror used for the two-port measurement

Pads	**Description**	**Location**	$\mathbf{C_{SIM}}$
Rotor Pad	Connected to GND & Port 1	North	-
Fast Axis Drive Pads	Two Pads to drive Inner Axis	South	11pF
Fast Axis Sense Pads	Four Pads to sense Inner Axis	East/ West	8.6pF
Slow Axis Drive Pads	Two Pads to drive Outer Axis	South	9.5pF
Slow Axis Sense Pads	Four Pads to sense Outer Axis	East/ West	16.8pF

2.3 Two-Port Measurement

For the two-port measurement the first port of the VNA is soldered to the rotor pad, as in Fig. 2 and the second port is soldered to one of the other pads, described in Tab. 1. The VNA is two-port calibrated, where the two SMA cables to the ports are included. In a next step the $S21$ parameter is measured with the VNA between the two ports, which is the insertion loss, as S-parameters are commonly used for impedance evaluations.[12] As the DUT is connected between the ports, a series-thru measurement is executed and the insertion loss $S21$ is calculated via a voltage divider as

$$S21 = \frac{2 \cdot Z_0}{2 \cdot Z_0 + Z_{DUT}} , \tag{1}$$

where Z_0 is the impedance of the ports, which have a value of 50 Ohm and Z_{DUT} is the impedance of the DUT. Therefore Z_{DUT} could be determined by

$$Z_{DUT} = 2 \cdot Z_0 \cdot \left(\frac{1}{S21} - 1 \right) , \tag{2}$$

for the different connections between the pads and the rotor pad by measuring the insertion loss $S21$. The measurement is executed for a frequency range of 1MHz up to 1GHz and the magnitude of $S21$ is saved in decibel over the entire range together with the phase in order to be able to calculate the impedance at different frequencies afterwards.[12]

3. RESULTS

All measurements have been carried out for three intact mirrors, two slightly broken mirrors and two severely broken mirrors. For the slightly broken mirrors only the springs of the inner axis were broken, while for the severely broken mirrors cracks did also propagate into the mirror plane. First the insertion loss $S21$ was measured in decibel over the logarithmic frequency range between the different pads and the rotor pad, where the averaged results could be seen in Fig. 3a for the intact mirrors. In a next step the impedance Z_{DUT} was calculated with Eqs. (2) with the measured $S21$ magnitude and phase values over the frequency range for the intact mirrors. It was determined that the imaginary part of Z_{DUT} is negative until approximately 300MHz and therefore the impedance is resistive and capacitive for this range. The resistance is the real part of the impedance, while the capacitance C_{DUT} could be calculated with the imaginary part and is shown in Fig. 3b over a frequency from 1MHz to 100MHz for the intact mirrors. In Tab. 2 the $S21$ values in decibel for different frequencies for the evaluated pads are shown, as well as the capacitance C_{DUT} values at 10MHz and 100MHz.

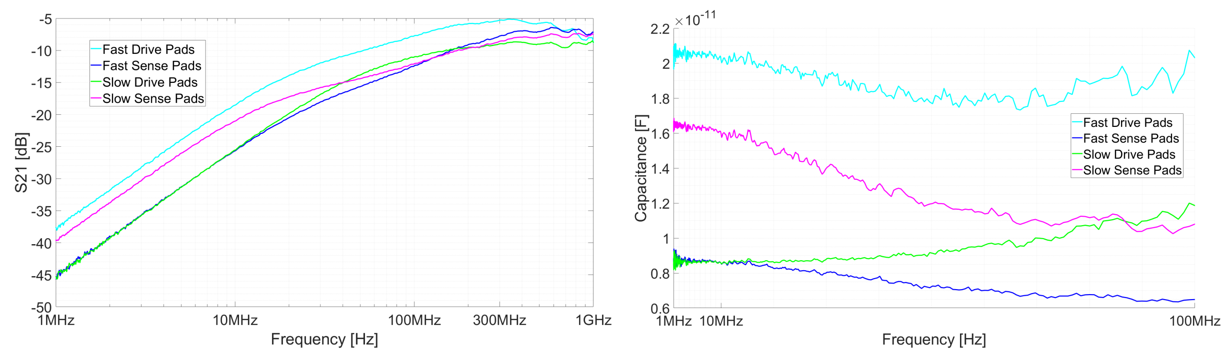

Figure 3. (a) Insertion loss $S21$ over logarithmic frequency for different pads averaged for the three measured intact mirrors. (b) Calculated capacitance C_{DUT} over logarithmic frequency for the different pads of the measured intact mirrors.

Table 2. Insertion loss $S21$ in dB and capacitance C_{DUT} values for the measured pads averaged for the intact mirrors for different frequencies

Pads	**1MHz**	**10MHz**	**100MHz**	**300MHz**	**1GHz**	C@**10MHz**	C@**100MHz**
Fast Drive Pads	-37.5dB	-18.5dB	-7.5dB	-5dB	-8dB	20.2pF	20.4pF
Fast Sense Pads	-45dB	-25.5dB	-12dB	-7.5dB	-7dB	8.6pF	6.6pF
Slow Drive Pads	-45dB	-25.5dB	-11dB	-8.5dB	-8.5dB	8.6pF	12pF
Slow Sense Pads	-39.5dB	-21dB	-12dB	-8.5dB	-7dB	16pF	10.6pF

The C_{DUT} values from Tab. 2 could be compared to the simulated values C_{SIM} in Tab. 1 now. For most of the pads the calculated C_{DUT} values from the measured $S21$ values at 10MHz match quite well with the simulated ones. For example, for the fast sense pads the simulated capacitance is 8.6pF, which is the same as the calculated. For the slow sense pads the simulated capacitance is 16.8pF and the calculated 16pF, which matches too. Moreover the simulated capacitance for the slow drive pads is 9.5pF and approximately matches with the calculated, which is 8.6pF. Finally the calculated capacitance for the fast drive pads has the largest deviation from the simulated one, which was 11pF. In a last step the same measurements were executed for two slightly and two severely broken mirrors, where again the insertion loss $S21$ was measured and the impedance was calculated and divided into capacitive and resistive part. The slightly broken mirrors were damaged at the inner axis springs, while the severely broken mirrors were broken at the inner springs and the cracks propagated into the mirror plate and other parts of the structure. In Fig. 4 the insertion loss $S21$ is shown for the intact mirrors in comparison to the first severely broken mirror, where deviations are visible especially for the fast drive and slow sense pads.

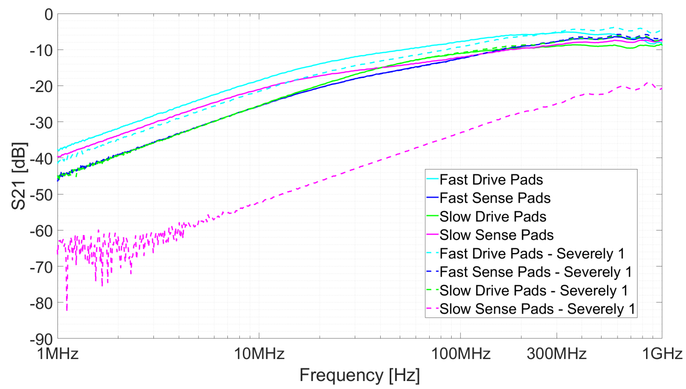

Figure 4. Insertion loss $S21$ over logarithmic frequency for different pads of intact mirrors and first severely broken mirror.

Table 3. Comparison of impedance Z_{DUT} values for the measured pads of intact and broken mirrors at 10MHz

Pads	**Intact**	**Slightly 1**	**Slightly 2**	**Severely 1**	**Severely 2**
Fast Drive Pads	20.2pF	19.5pF	17.7pF	15pF	17.3pF
Fast Sense Pads	8.6pF	8.1pF	7.6pF	7.5pF	7.2pF
Slow Drive Pads	8.6pF	8.6pF	8.6pF	8.4pF	**1pF**
Slow Sense Pads	16pF	15.8pF	15pF	**5.6pF**	14.2pF

In Tab. 3 the capacitance C_{DUT} results at 10MHz for slightly and severely broken and intact mirrors are compared to each other in order to determine differences due to the breakage of the mirror structures. It is shown that for slightly broken mirrors only small differences are visible in the capacitance for the fast axis drive and sense pads due to the breakage of the springs on this axis. These capacitance deviations are difficult to distinguish from measurement variations between mirrors and due to soldering, which are around 0.5pF to 1pF. On the other hand it could be seen that the capacitance for the first severely broken mirror is much smaller for the fast sense and drive pads, as well as for the slow sense pads. Therefore the propagated cracks do not only influence the impedance of the inner axis, but also the impedance of the outer axis sense pads, as most likely interconnect tracks were damaged. In addition to that the capacitance of the second severely broken mirror shows large deviations for the slow axis drive pads in addition to slight deviations for the fast axis drive and sense pins, probably due to propagated cracks.

4. CONCLUSION

In conclusion the results of the proposed failure detection method with two-port measurements for impedance evaluation showed, that there are capacitance differences visible between broken and intact MEMS mirrors. For slightly broken mirrors, where only the inner springs were damaged, the deviations in capacitance were quite small and difficult to distinguish to measurement variations between different mirrors, which were approximately around 0.5pF to 1pF. On the other hand the capacitance deviations for severely broken mirrors were larger and did also affect the outer axis, which was not visibly broken, due to the propagation of cracks from the breakage of the inner axis. Therefore such severe breakages of mirrors could be detected with the help of the described impedance measurements, as the variations are large compared to measurement deviations. Hence, the proposed concept is applicable for failure analysis after a severe breakage has occurred for a mirror. In order to detect breakages for slightly broken mirrors, a more precise measurement method is needed with smaller variations. In addition the capacitance results for intact mirrors were compared to simulation results and match quite well with them for most of the measured pads. As an outlook the measurement could be executed for a larger number of mirrors in order to gather more statistical data and the crack propagation could be investigated. Moreover in order to detect slightly broken mirrors a more precise impedance measurement method could be investigated and it could be tried to measure the impedance of MEMS mirrors during operation and breakage to compare the results.

ACKNOWLEDGMENTS

The authors would like to thank ARCHIMEDES, which is supported by the Chips Joint Undertaking and its members, including the top-up funding by National Authorities under Grant Agreement No 101112295. This work was supported by the project ARCHIMEDES, which is funded by the European Union. Views and opinions expressed are however those of the author(s) only and do not necessarily reflect those of the European Union or the granting authority. Neither the European Union nor the granting authority can be held responsible for them. Thank goes also to Simon Waldhuber, Benedikt Kraxner and Christoph Maier.

REFERENCES

[1] T. Tsuchiya, "MEMS mirrors for automotive applications," 2017 IEEE International Meeting for Future of Electron Devices, Kansai (IMFEDK), Kyoto, Japan, pp. 82-83, (2017).

[2] N. Druml, P. Greiner, I. Maksymova and L. Niedermuller, "Sense and control of oscillating MEMS mirrors," 25th Euromicro Conference on Digital System Design (DSD), Maspalomas, Spain, pp. 726–732, (2022).

[3] I. Maksymova, P. Greiner, J. Wiesmeier, F. M. Darrer and N. Druml, "A MEMS mirror driver ASIC for beam-steering in scanning MEMS-based LiDAR," in Laser Beam Shaping XIX, Proc. SPIE 11107, (2019).

[4] N.Druml, I. Maksymova, T. Thurner, D. v. Lierop, "1D MEMS microscanning LiDAR" International Conference on Sensor Device Technologies and Applications, (2018).

[5] U. B. Sven, T. S. Holmstrom and H. Urey, "Mems laser scanners: A review," Journal of Mircoelectromechanical Systems, Vol. 23, no. 2, (2014).

[6] P. Rafiee, G. Khatibi and M. Zehetbauer, "A review of the most important failure, reliability and nonlinearity aspects in the development of microelectromechanical systems (MEMS)," Microelectronics International, Vol. 34, Issue 1, pp. 9–21 (2017).

[7] M. T. Jan, N. H. B. Hamid, M. H. M. Khir, K. Ashraf and M. Shoaib, "Reliability and fatigue analysis in cantilever-based MEMS devices operating in harsh environments," Journal of Quality and Reliability Engineering, (2014).

[8] B. Caillard, Y. Mita, Y. Fukuta, T. Shibata and H. Fujita, "A highly simple failure detection method for electrostatic microactuators: Application to automatic testing and accelerated lifetime estimation," IEEE transactions on semiconductor manufacturing, vol. 19, no. 1, (2006).

[9] W. Ma, H. -Y. Chan, C. C. Wong, Y. C. Chan, C. -J. Tsai and F. C. S. Lee, "Design optimization of MEMS 2D scanning mirrors with high resonant frequencies," 2010 IEEE 23rd International Conference on Micro Electro Mechanical Systems (MEMS), Hong Kong, China, pp. 823-826, (2010).

[10] P. Deng and W. Ma, "Nonlinearity investigation of the MEMS scanning mirror with electrostatic comb drive," The 9th IEEE International Conference on Nano/Micro Engineered and Molecular Systems (NEMS), Waikiki Beach, HI, USA, pp. 212-215, (2014).

[11] H. Schenk, P. Durr, D. Kunze, H. Lakner and H. Kuck, "An electrostatically excited 2D-micro-scanning-mirror with an in-plane configuration of the driving electrodes," Proceedings IEEE Thirteenth Annual International Conference on Micro Electro Mechanical Systems, Miyazaki, Japan, pp. 473-478, (2000).

[12] S. M. Sandler, "Power Integrity : Measuring, optimizing, and troubleshooting power related parameters in electronics systems," First edition, McGraw-Hill Education, New York, pp. 21-23, (2014).